

Flow and Sediment Transport Simulation in River Channels and Around Weirs: A Computational Analysis Using MIKE and FLOW3D

Teammates: Pan Xinxin (Leader), Wang Yalin, Zhao Lingzhen, Tang Jiatong

Abstract:

This study investigates the optimization of the Shawan River channel in Shenzhen, including channelization and overflow weirs, to enhance flood protection and stabilize flow. Using MIKE and FLOW3D models, we analyze the performance of both natural and widened channel configurations under various flow conditions. The results show that the optimized channel improves both stability and hydraulic efficiency, as demonstrated through a comparison of the minimum Froude number. A comparison of trapezoidal weirs with varying upstream slopes reveals that milder slopes increase flow capacity, whereas steeper slopes increase shear stress and bedload transport, further enhancing the risk of bed erosion and the formation of scour holes. These findings provide valuable insights for effective river training and channel design.

Keywords:

Stable Flow; Turbulence; Sediment Transport; Weir Shape.

1. Introduction

In river training and channel design, several critical principles must be followed to achieve the dual objectives of enhancing flood protection and stabilizing flow [1]:

- 1) Increase the average channel width;
- 2) Decrease the average flow depth and velocity to balance sediment deposition and bed erosion;
- 3) Installing overflow weirs to manage sediment transport, regulate flow velocity, and control discharge.

The best way to identify whether a channel is in equilibrium is its stability. A stable channel is considered to be in equilibrium, characterized by the absence of systematic erosion or deposition. Therefore, the highest level of stability in an alluvial river channel signifies its equilibrium. Engineers typically achieve flow stability by adjusting channel width, and use a key indicator – minimum Froude number – to reflect maximum channel stability in Jia's study [2].

Another measurement is building overflow weir. Occurrence of overflow weir alters the river's width, which results in flow separation around it and leads to circumfluence downstream, where the water swirls or circulates due to the disturbance in the flow pattern. [3] As the streamlines are compressed and velocity increases, the riverbed around weirs experiences significant scouring, leading to the formation of scour holes. The turbulence around weirs constitutes a complex fluid–structure interaction (FSI) and sediment transport problem. Numerical models and CFD tools have been used in this issue over the years.

We validate these design principles using a river channelization case of Shawan River Regulation Project (2016)[4], and compare hydraulic characteristics of the 900m-long river channel (Chainage: S3+570.21 ~ S4+470.05) (See Fig. 1) before and after the implementation (See Fig. 2 and Fig. 3) of the project. The Shawan River is part of the Pearl River Delta Basin, a crucial watershed in Shenzhen.

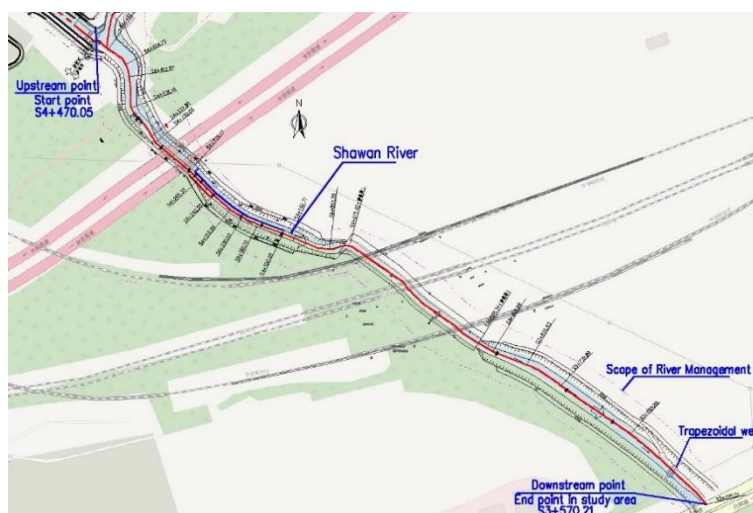


Fig. 1. Selected 900-meter-long channel in Shawan River

The Shawan River Regulation Project implemented several measures:

- 1) Expanding the channel's bottom width;
- 2) Channelizing channel cross-sections into a trapezoidal form;
- 3) Installing submerged trapezoidal weirs to manage sedimentation and optimize flow velocity and discharge.

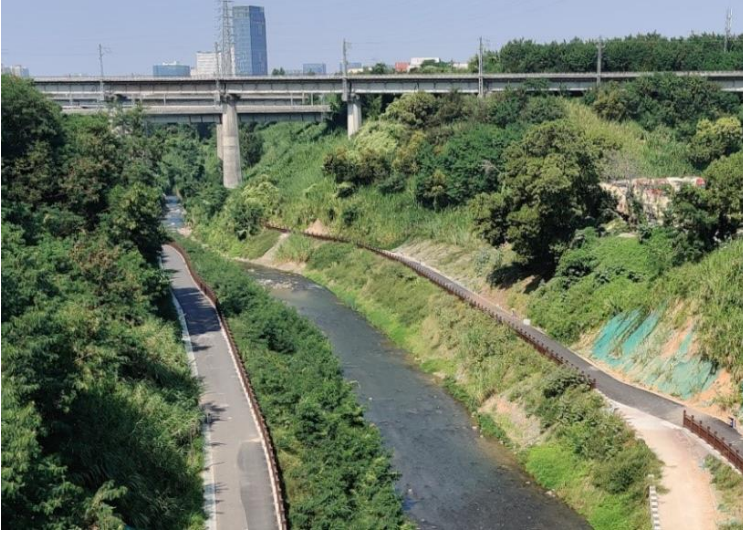


Fig. 2 Post-implementation



Fig. 3 A long-term averaged flow state in weir

This study evaluates these principles with a focus on hydraulic properties and sediment transport, including:

- 1) Modelling flow conditions in the natural versus widening channels in MIKE 11;
- 2) Determination of the appropriate upstream slope for weirs, considering the asymmetry of the weir cross-section; simulating various cases in FLOW3D.

2. Methodology

2.1. Flow Computation in Channels

2.1.1. Hydrological Model

DHI MIKE is one of the most widely used hydrodynamic models. It is used to simulate water surface profiles and discharge in rivers. [5] It solves the Saint-Venant equations, which describe the conservation of continuity and momentum, allowing for the simulation of fully dynamic wave behavior.

In MIKE 11, a network configuration depicts the rivers and floodplains as a system of interconnected branches. The discharge-water level relationship ($Q-h$) is selected as boundary condition to model equilibrium flow, that is specified when the relationship between the discharge and the water level is known (HD model). Modelling requires several data inputs, including a topographic map of the study area, river geometry, and time series data for water levels and discharge.

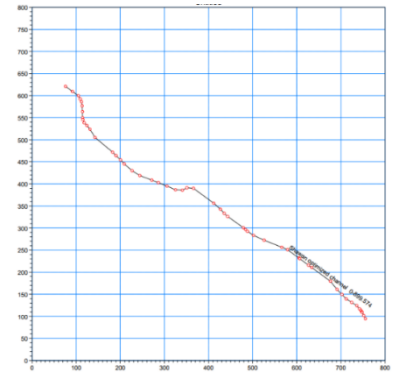


Fig. 4. River network in MIKE

2.1.2. Flow Condition and Input Setup

Three flow conditions were modeled for analysis:

- 1) **Natural Channel:** Extreme discharge of $Q=200m^3/s$ at the upstream boundary, representing a 100-year return period storm ($P = 1\%$), with corresponding initial water levels at the downstream boundary; natural river geometry seen gray dotted line in Fig. 5.
- 2) **Optimized Channel:** Same boundary conditions as scenario 1, with channelization trapezoidal cross-sections (See red line in Fig. 5).

- 3) **Natural Channel:** Long-term averaged discharge of $Q=50m^3/s$ at the upstream boundary ($P=50\%$), with corresponding water level at the downstream boundary.

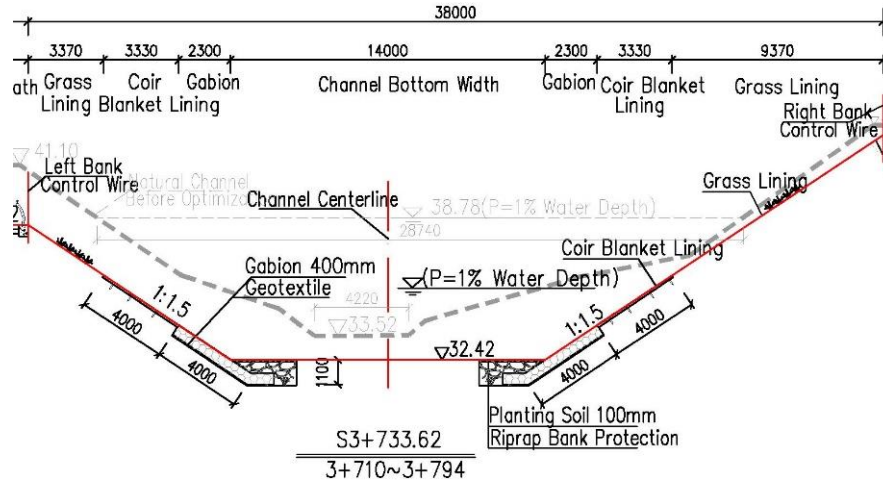


Fig. 5. Optimization channel section

The river geometry was defined by inputting cross-sections at approximately 50-meter intervals along the channel.

Considering the different Manning's coefficient n , $n=0.030$ for Natural channel with sand bed, and $n=0.025$ for optimized channel with Coir Blanket Lining Bank (See Fig. 5).

2.1.3. Froude Number

The Froude number (Fr) is generally calculated using the following equation:

$$Fr = \frac{V}{\sqrt{gh}} \quad (2-1)$$

Where:

- V is the flow velocity,
- g is the acceleration due to gravity, and
- h is the flow depth.

From Jia's study, [2] the ideal minimum value of the Froude number (Fr_{min}) can be determined through simulation. These simulations are based on several key assumptions:

- 1) The sand-bed river channel is alluvial.
- 2) Adjustments to the slope and cross-sectional shape of the channel must satisfy the equilibrium conditions for water and sediment transport.
- 3) These adjustments are related to the resistance provided by bed forms and sediment particles to the flow.

In this project, a minimum value of Fr can be calculated from the simulation results,, which corresponds to a particular set of hydraulic geometry parameters. For other variables, such as stream power per unit length (slope) and per unit weight of water, as well as flow resistance, no minimum values were found. However, the minimum Froude number (Fr_{min}) represents a unique and stable equilibrium state of the highest stability. According to the analysis, this minimum Froude number indicates the most stable equilibrium condition for the system.

From Jia's laboratory tests, the following regression equation for Fr_{min} was derived:

$$Fr_{min} = K \times (V \times J)^b \quad (2-2)$$

Where:

- b is almost constant;
- K differs according to the size of sediment;
- J is the slope.

The values of b and K can be considered constant for a given sediment type, with K depending on the sand and gravel diameter d . From the laboratory tests, the relationship between K and d was obtained as follows (Fig. 6).

$$K = 4.49 \times d^{-0.186} \quad (2-3)$$

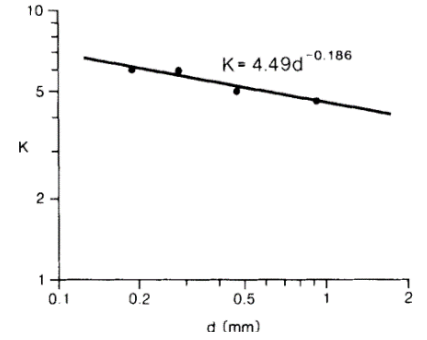


Fig. 6 The relation of K to d

Thus, the final formula for Fr_{min} in this case is:

$$Fr_{min} = 4.49 \times d^{-0.186} \times (VJ)^b \quad (2-4)$$

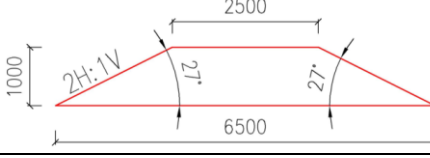
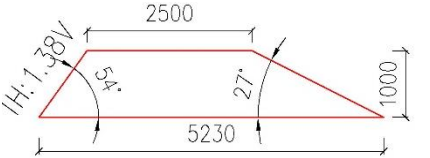
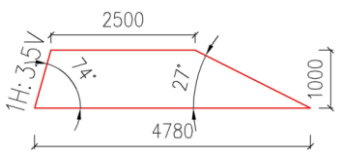
2.2. Configuration and Numerical Setup for Weirs

This study employs numerical simulations and corresponding case comparisons to analyze flow performance around weir.

2.2.1. Flow and Weir Condition

To evaluate the impact of asymmetry in weir design on flow efficiency, three upstream weir slopes (θ) were selected based on reference tests[6]: 27° , 54° and 74° . Additionally, the weir height (Z) was set at 1 m, the weir crest length (L_{cr}) at 2.5 m, and the downstream slope (θ_d) at 27° . These parameters represent an optimized design configuration (See Table. 1 for detailed weir design parameters and sketches).

Table. 1. Geometrical Conditions of Weirs

Weir No.	Weir section	Upstream slope θ	Upstream H:V	Weir Length(m)
1		27°	1:0.5	6.50
2		54°	1:1.38	5.23
3		74°	1:3.5	4.78

The simulated channel has a total length of 30 meters, with a fixed distance of 10 meters ($L_1=10m$) between the upstream weir and the channel's starting point. A submerged flow condition was modeled with a water depth of $H_0=1.5m$ to simulate a discharge of $Q=50m^3/s$ ($P=50\%$ corresponds to a long-term average water level). The initial water depth was set to 0.75 meters, which is 0.25 meters lower than the weir crest, to highlight the water-surface profile.

The downstream portion of the channel was modeled with a bottom width of 14 meters.

2.2.2. Numerical Setup

Numerical simulations of Weir1~3 were performed to analyse the free water surface, the flow velocity (u , v , and w) and turbulence condition around weirs.

The FLOW-3D computational fluid dynamics (CFD) code was used for the simulations. This software utilizes the finite volume method to solve the Reynolds-averaged Navier-Stokes (N-S) equations and employs the Volume of Fluid (VOF) method to track free surface[7].

The Renormalization Group (RNG) turbulence model was employed to manage turbulent viscosity and prevent excessive values.

- **RNG k- ϵ model**

The k- ϵ model generally describes turbulence by means of two PDEs, and there are two corresponding variables: 1) the turbulent kinetic energy (k); 2) the rate of dissipation of turbulent kinetic energy (ϵ). It is widely used in commercial CFD software FLOW3D to simulate mean flow characteristics for turbulence.

1) k equation:

$$\frac{\partial k}{\partial t} + u_i \frac{\partial k}{\partial x_i} = \frac{\partial}{\partial x_i} \left(\frac{v_i}{\sigma_k} \frac{\partial k}{\partial x_i} \right) + v_t \left(\frac{\partial u_i}{\partial x_j} + \frac{\partial u_j}{\partial x_i} \right) \frac{\partial u_i}{\partial x_j} - \epsilon \quad (2-5)$$

2) ϵ equation:

$$\frac{\partial \epsilon}{\partial t} + u_i \frac{\partial \epsilon}{\partial x_i} = \frac{\partial}{\partial x_i} \left(\frac{v_i}{\sigma_\epsilon} \frac{\partial \epsilon}{\partial x_i} \right) + c_{\epsilon 1} \frac{\epsilon}{k} p - c_{\epsilon 2} \frac{\epsilon^2}{k} \quad (2-6)$$

The turbulence intensity I is a key indicator to evaluate the turbulence downstream of the weirs, calculated as follows:

$$I = \sqrt{\frac{k_T}{\bar{K}}} \quad (2-7)$$

where k_T is the turbulent kinetic energy, \bar{K} is the mass-averaged mean kinetic energy in the domain.[7]

To optimize computational efficiency, a structured and mixed orthogonal mesh was used. Smaller cells (0.25 m) were applied in the weir region, while larger cells (0.5 m) were applied in the upstream and downstream sections (See Fig. 7~8). The total number of cells exceeded 60,000 for the 30-meter-long computational domain.

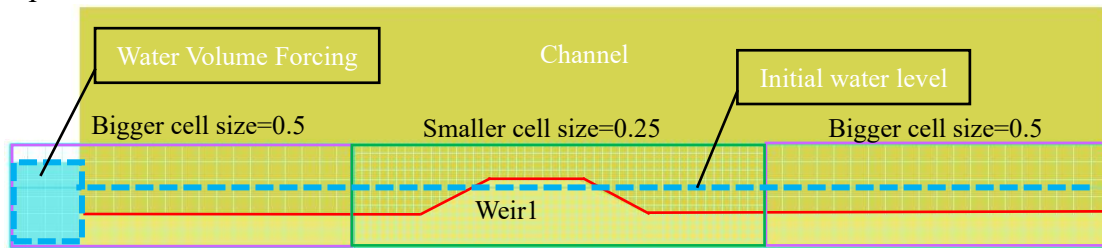


Fig. 7. Meshing in Y-Z Plane

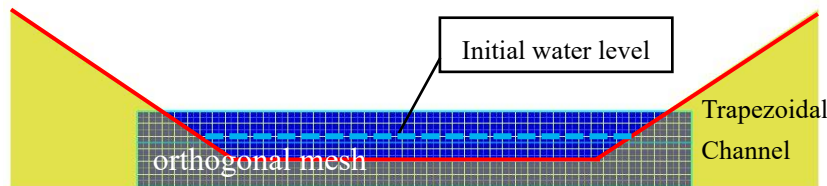


Fig. 8. Meshing in X-Z Plane

Flow data, including velocity and Froude number, were recorded at a specific location at the center of the weir along the Y-Z plane.

2.3. Bedload and Suspended Sediment Analytical Solutions

A MATLAB model framework for sediment transport within different discharges was conducted in bedload and suspended analysis, integrating implicit solutions for settling velocity, empirical formulations and depth-integrated equations.

2.3.1. Bedload Transport

Relative bed-load transport formula developed by Meyer-Peter & Müller (MPM), based on Shields number. [8]

- **Settling velocity w_s**

Settling velocity is defined by the equation giving equilibrium between gravity force and flow resistance, then obtain:

$$w_s = \sqrt{\frac{4(s-1)gd}{3c_D}} \quad (2-8)$$

Where:

- s is the relative density of natural sediments, $s = 2.65$,
- g is the acceleration due to gravity,
- d is diameter of sediment particle, in this case, diameter of natural sand $d = 0.2\text{mm}$,
- c_D is the drag coefficient, and $c_D = 1.4 + 36/R$,
- R is the grain Reynolds number, and $R = w_s * d / \nu$, and
- ν is kinematic viscosity, $\nu = 10^{-6} \text{ m}^2/\text{s}$.

- **The semi-empirical Meyer-Peter & Müller (MPM) method**

The non-dimensional quantity Φ_B within different theories and methods, then transfer it to the bed load transport rate q_B . Engineers prefer semi-empirical methods by MPM as it always falls within the intermediate range. [9]

$$\Phi_B = 8(\theta' - \theta_c)^{3/2} \quad (2-9)$$

where the critical shield parameter θ_c and the Reynolds number Re is calculated by following:

$$\theta_c = 0.165(Re + 0.6)^{-0.8} + 0.045e^{-40Re^{-1.3}} \quad \text{for } Re \geq 1 \quad (2-10)$$

$$Re = \frac{U_f v}{\nu} \quad (2-11)$$

where U_f is the shear velocity (friction velocity), v is mean velocity, that are calculated in FLOW.

The transformation between bedload transport rate and non-dimensional quantity is:

$$q_B = \Phi_B \times \sqrt{(s-1)gd} \quad (2-12)$$

- **Effective Shields Numbers**

Engelund and Fredsøe (1982) [8] recommend the following empirical relationships for effective Shields parameter θ' in the lower or upper regime:

- 1) For the upper regime ($\theta' > 0.55$): $\theta' = [0.702\theta^{-1.8} + 0.298]^{-1/1.8}$;
- 2) For the lower regime ($\theta' \leq 0.55$): $\theta' = 0.3\theta^{1.5} + 0.06$.

2.3.2. Shields Regime Diagram

Garcia (2000) presents the Shields regime diagram (SRD) is seen in Fig. 9, which can be used to differentiate sediment movement patterns. [11] The suspension concentration and conditions near the bedform can be analyzed using the effective Shields parameter θ' and the particle Reynolds number R_p in the SRD, where R_p and dimensionless shear stress $\tau^* = \theta'$ can be calculated from the hydraulic

and sediment characteristics of the given flow.

$$\theta' = \tau' = \frac{\tau'}{\rho g(s-1)d} \quad (2-13)$$

where the problem of estimating the effective shear stress τ' has not yet been solved in a completely explicit way.

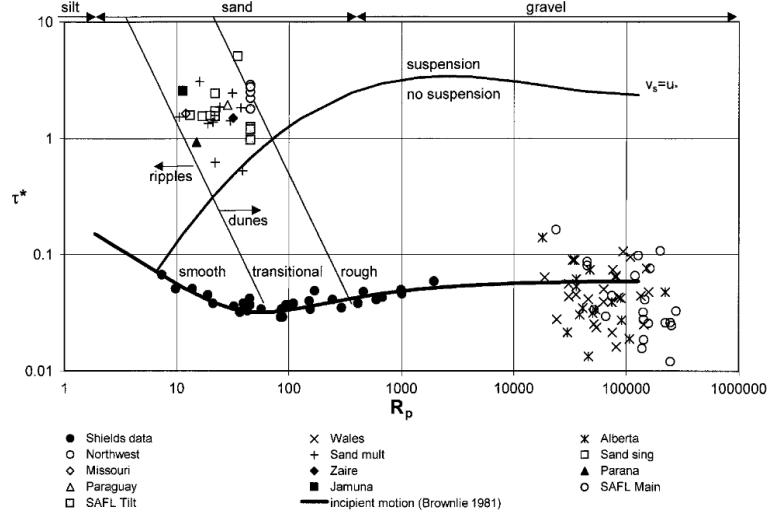


Fig. 9 Shields regime diagram and critical Shields' data by Brownlie

Garcia referred to the curve where $U_f = w_s$ for sand spheres as the transition between suspension and no-suspension of sediment particles in the SRD.

2.3.3. Suspended Sediment

For fine sediment particles, the critical parameters can be explicitly defined[10] using the particle Reynolds number R_p , calculated as:

$$R_p = \frac{Re}{\sqrt{\theta}} = \frac{\sqrt{(s-1)gd}d}{v} \quad (2-14)$$

where R_p depends (among other things) on the sediment size d , but not other hydro-dynamic factors.

Then, the dimensionless Shields parameter θ is expressed as:

$$\theta = \frac{Uf^2}{(s-1)gd} \quad (2-15)$$

3. Analysis and Discussion

3.1. Velocity Assessment in Channels

This analysis focuses on velocity distribution at 14 selected locations within the channel. Using MIKE11 software, the Froude number for the natural (present) condition (Fr_{pre}) and the widening (optimized) condition (Fr_o) are obtained from the water depth and flow velocity data.

• Minimum Froude Number

Based on the available information for the Shawan River, the sand and gravel diameter $d = 0.2 \text{ mm}$, which results in a b -value of about 0.377, as derived from JIA's work [2]. Use Equation(2-3), the K value was calculated as: $K = 4.49 \times 0.2^{-0.186} = 6.057$.

From the design report, the average slope J of the channel is given as 0.002. Based on simulation results, the velocity V at the 14 locations in the natural state was calculated, yielding an average

velocity $V_{\text{mean}} = 1.86\text{m/s}$.

Table. 2. Flow features form simulating results

Chainage	Slope J	V
0	0.002	0.911
76.45	0.002	0.993
93.95	0.002	1.03
122.05	0.002	0.946
191.05	0.002	2.573
230.05	0.002	1.64
320.05	0.002	2.525
406.45	0.002	1.933
453.04	0.002	2.255
494.72	0.002	2.105
581.71	0.002	2.435
633.73	0.002	2.33
736.43	0.002	2.043
844.05	0.002	2.304
Mean velocity		1.86

Therefore, the ideal minimum Froude number of Shawan River ($Fr_{\text{min_SW}}$) is:

$$Fr_{\text{min_SW}} = 6.057 \times (VJ)^{0.377} = 0.735$$

Comparing the results with the design standards from the Code of Practice on Surface Water Drainage in Singapore [12], which suggests a design Froude number of 0.8, we find that Fr_{min} is very close to this standard. According to JIA's study[2], Fr_{min} represents the most stable condition of the channel. Therefore, $Fr_{\text{min_SW}}$ can be considered an appropriate stability indicator for the study area, representing the river channel's most stable state.

From simulations, the flow profiles and Fr numbers are shown below.

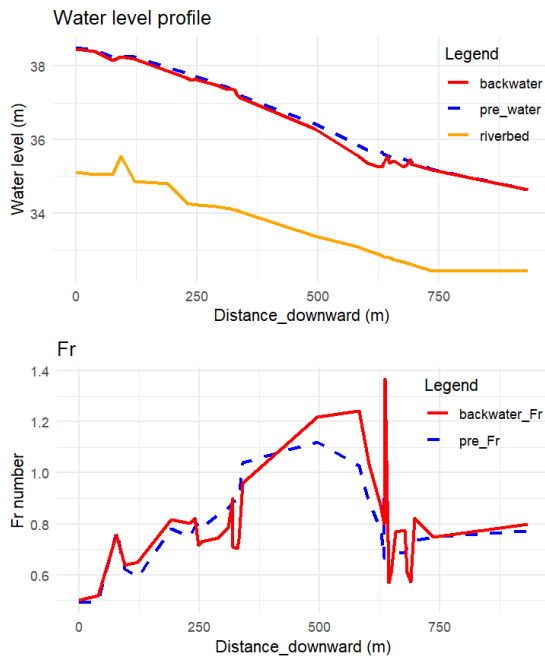


Fig. 10 Velocity and Fr profile

Table. 3. Calculation of Fr

Distance	Fr_pre	Fr_o
0	0.39	0.64
76.45	0.41	0.93
93.95	0.53	0.54
122.05	0.63	0.78
191.05	1.27	0.9
230.05	1.14	1.15
320.05	0.95	1.33
406.45	1	0.83
453.04	1.37	0.99
494.72	1.17	1.01
581.71	1.14	1.33
633.73	0.87	0.88
736.43	0.77	0.96
844.05	0.83	1

The optimization effects were analyzed by comparing $Fr_{\text{min_SW}}$, Fr_{pre} and Fr_{o} with respect to

performance indicators. The following graph shows the variance analysis along the downstream flow direction.

Upon analyzing the boxplot in Fig. 11, several key observations can be made:

- 1) The distribution of Fr_o is more concentrated, with 75% of the values below 1, indicating a more stable flow condition that avoids prolonged supercritical flow.
- 2) The distribution of Fr_{pre} is significantly more dispersed, with approximately 30% of the values exceeding 1, indicating highly unstable flow conditions.
- 3) The median of Fr_o shows a lower variance in the stability index compared to Fr_{pre} , although it remains close.

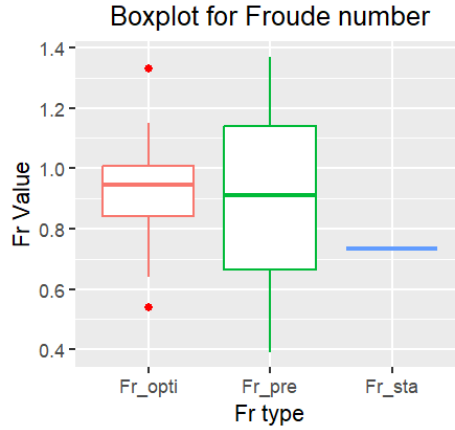


Fig. 11 Boxplot for Comparison of Fr

From this statistical analysis, it can be concluded that the optimized channel demonstrates improved stability compared to the natural channel.

3.2. Overflow Weirs

This section examines submerged trapezoidal broad-crested weirs under varying upstream face slopes, focusing on long-term average water level flow conditions. The flow behavior observed is as follows: upstream of the weir, the flow is subcritical ($Fr_1 < 1$); over the weir crest, a critical flow transition occurs; and downstream, the flow becomes supercritical ($Fr_2 > 1$), eventually returning to subcritical flow further downstream.

The simulation results presented below illustrate these flow properties through graphs and charts.

3.2.1. Flow Surface Profile

The computed free surface elevation is used to plot the streamlines over the three types of weirs under constant discharge conditions (See Fig. 12). The water surface profile at the downstream end of the weir depends on the initial water level and is not the primary focus of this analysis.

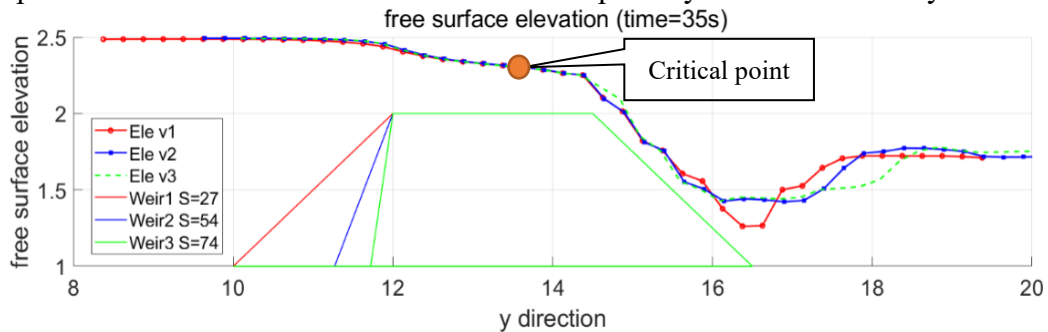


Fig. 12. computed water-surface profile over the weirs

In practice, undular flow can lead to pressure redistribution and potential damage to hydraulic structures, a condition that must be avoided in river engineering. The Froude number along the stream (See in Fig. 12) demonstrates that the current weir design avoids the formation of undular flow. This can be confirmed by applying the criterion for undular flow formation [13]:

$$\frac{H_0 - Z}{L_{cr}} < 0.15 \quad (3-1)$$

where numerator $H_0 - Z$ represents the upstream head above the weir crest, and the weir crest length $L_{cr}=2.5m$. In this case:

$$\frac{H_0 - Z}{L_{cr}} = 0.2 < 0.5 \quad (3-2)$$

that indicating that the flow over the weir typically forms a parallel streamline. Notably, as the slope (θ) increases, the hydraulic jump downstream shifts further away from the weir heel.

3.2.2. Critical point

The weir effectively controls the discharge, causing the flow over the weir to transition into a supercritical state (See Fig. 13).

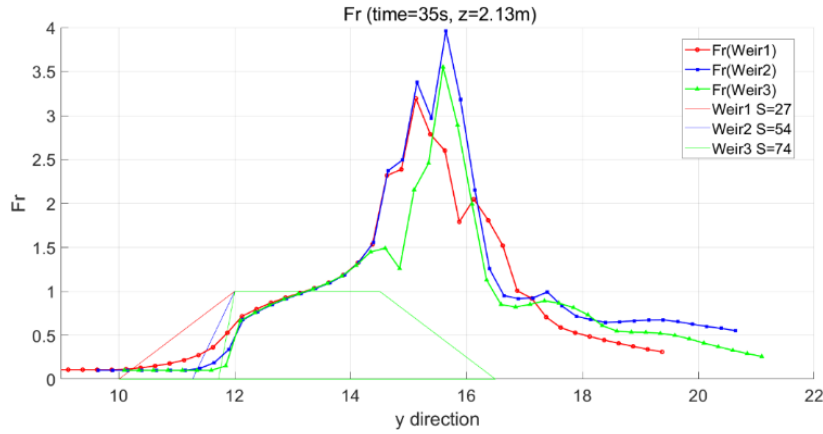


Fig. 13. Froude number along the stream

The first transition to critical flow occurs on the crest, and the upstream slope does not significantly alter the location of this transition. The Froude number reaches its peak near the weir heel. When combined with the water profile, it is evident that Weir 2, which has a higher Fr , exhibits faster velocity and lower water depth, potentially increasing the risk of bed scour.

3.2.3. Velocity distribution

Error! Reference source not found. illustrates the velocity distribution by 3D velocity magnitude, with the maximum vertical velocity values extracted in **Error! Reference source not found.**

The overall velocity distribution along the streamline can be described as follows:

- 1) Upstream of the weirs, the velocity profiles are straight and uniform.
- 2) Flow velocity gradually increases as the water reaches the weirs. Compared to mild upstream slopes, a steeper slope results in a sharp velocity increase at the corner of the weir. Steep slopes or shallow water depths cause the flow to slow significantly behind the weir, leading to water accumulation and reduced discharge over the weir. The discharge for submerged trapezoidal weirs in open channels can be calculated by:

$$Q = C_D B \sqrt{2gH}$$

where H is total overflow head, it can be illustrated that the steep slopes reduce the discharge coefficient C_D . [14]

Table. 4 Maximum vertical velocity along downstream face

Weir	Max w (m/s)	Distance to heel(m)
1	2.12	0.625
2	1.91	1.855
3	1.40	1.655

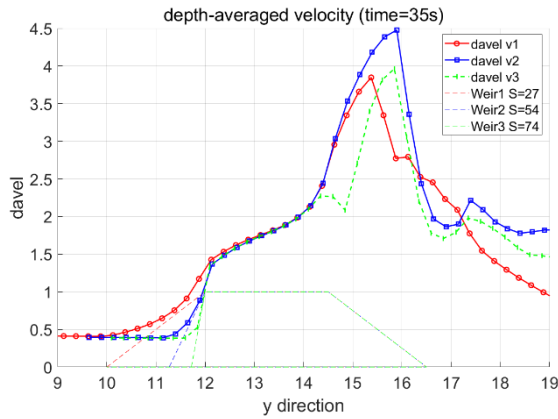


Fig. 15. Depth-averaged velocity (unit: m/s)

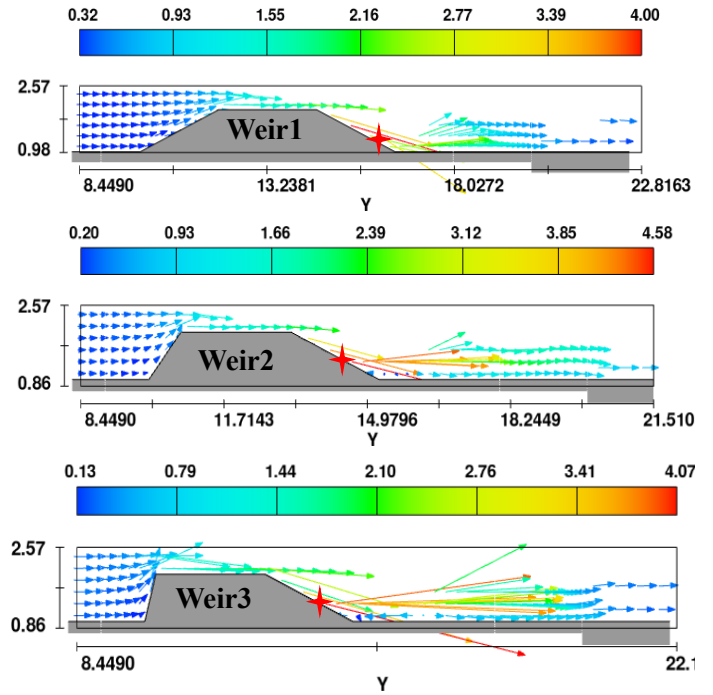


Fig. 14 Velocity distribution

- 3) Downstream of the weirs, the maximum vertical velocity typically occurs near the weir heel. Although mild slopes result in relatively lower average velocity magnitudes, they produce significantly higher vertical velocities. Conversely, steep slopes lead to minimal vertical velocity and relatively lower average velocity magnitudes.
- 4) Compare the flow velocity profile before and after weir in Fig. 16, where the downstream measurement distance is 2m from the heel. In the velocity profile after the Weir 3, a sudden change was observed.

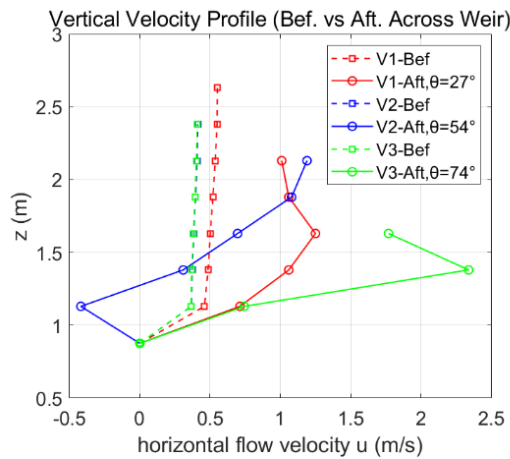


Fig. 16 Comparison of flow velocity profile before and after weir

- 5) Streamlines are compressed significantly and velocity increases in Weir3, with higher TKE compared to Weir1.

3.2.4. Turbulence Over Weirs

Turbulence typically occurs before and after weirs, causing energy losses, noise, and structural

vibrations. The optimal design of weirs aims to minimize these effects.

The results show that similar turbulence intensities occur downstream of all weirs (See Fig. 17), though Weir 3 (with a steep slope) produces a smaller turbulence range. This suggests that steeper slopes reduce turbulence and its associated negative effects.

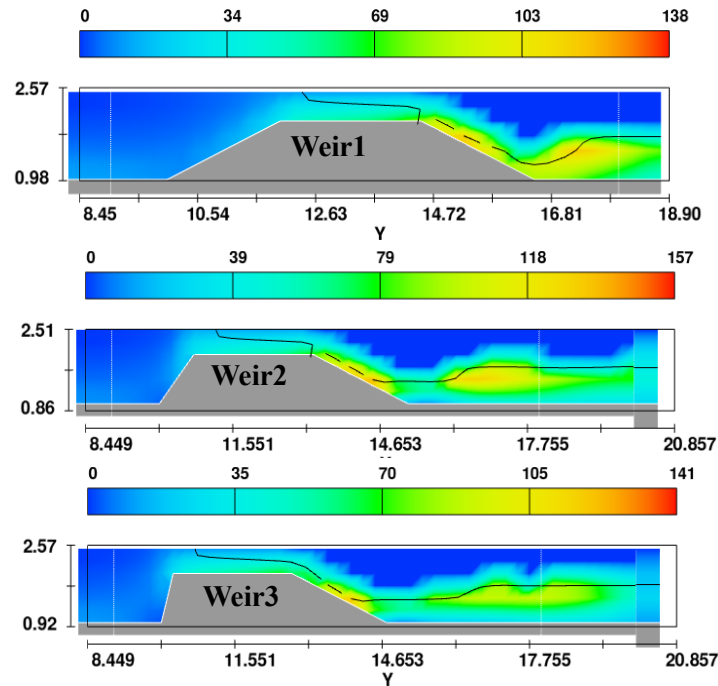


Fig. 17. Turbulence Intensity (unit: %)

3.2.5. Sediment Transport Analysis

Sediment transport is generally composed of two components: suspended load and bedload. In the Shawan Channel, the primary sediment is sand with $d=0.2mm$.

1) Bed-Load Sediment

Compared to gentler upslopes, Weir3 exhibits a significant shift in shear velocity and q_B . For Weir3 with a steeper upstream slope, although q_B is lower in the upstream, a rapid increase in downstream of the weir suggests a heightened potential for scour and erosion.

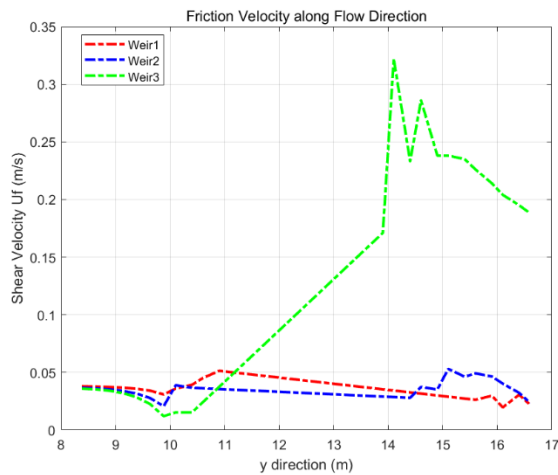


Fig. 18 Friction Velocity along Flow Direction

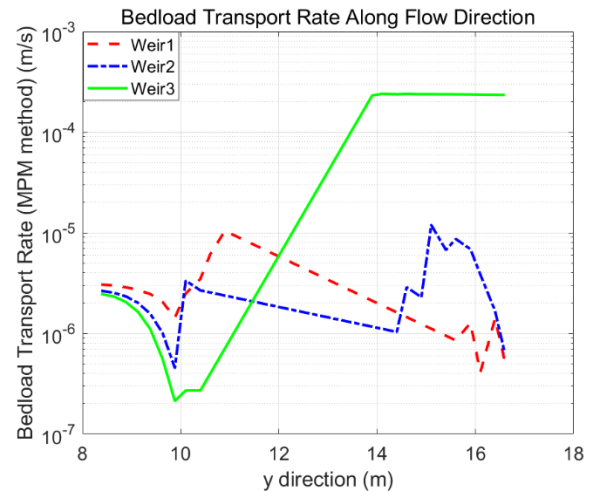


Fig. 19 Bedload Transport Rate (MPM method) q_B

Therefore, a steeper upstream slope of the weir stabilizes sediment before the weir, but may increase erosion and bed erosion near the heel, potentially leading to the formation of scour holes.

2) Simplified Analysis without Water Depth Consideration

The Hjulström-Sundborg diagram (Fig. 20) is a useful tool for understanding the erosion, transport, or deposition of sediment grains. However, it does not account for water depth.

Given that the sand in the Shawan River has a diameter of approximately $D=0.2\text{ mm}$ and the velocity downstream of the weir exceeds 1 m/s , erosion is highly probable. It's essential to recognize that while sedimentation results from velocity deceleration, erosion occurs due to velocity acceleration, which the Hjulström curves do not consider.

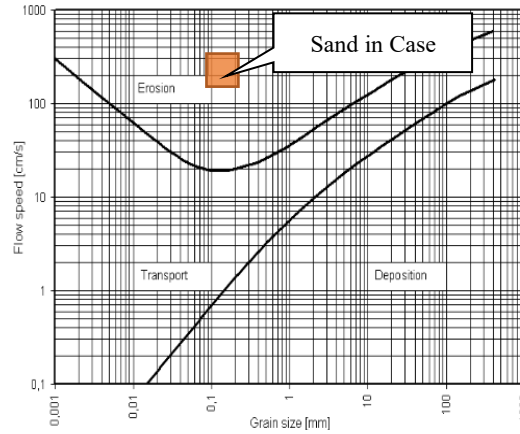


Fig. 20. Hjulström-Sundborg diagram

3) Suspension Sediment in SRD

Based on the analysis using the SRD (See in Fig. 21), the effective Shields numbers θ' exhibit a rapid increase at Weir3, indicating that sediment is in suspension over Weir3. The bedform transition from ripples to dunes typically occurs as flow conditions become deeper or more energetic, that may result in more erosion in the downstream riverbed.

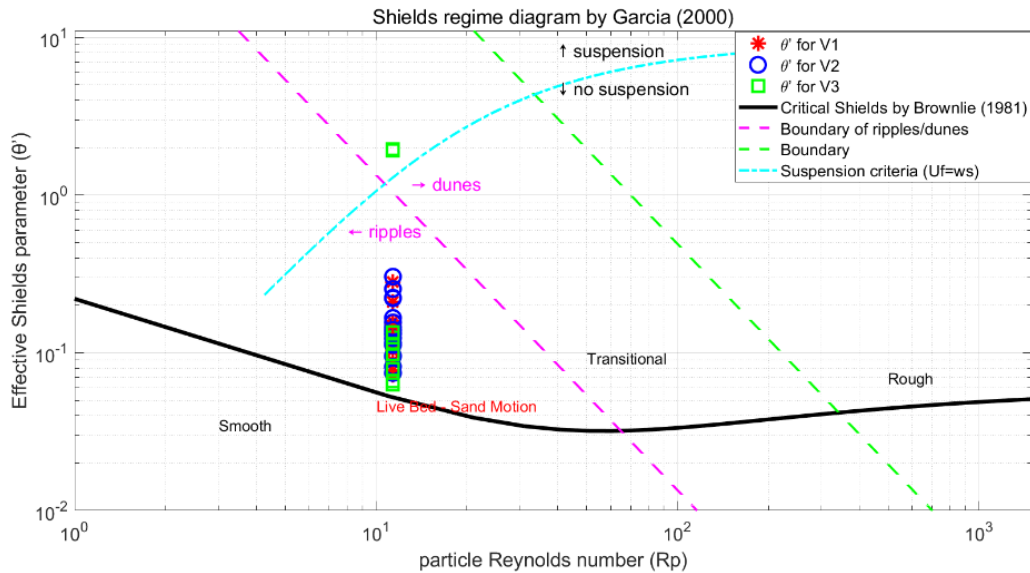


Fig. 21 Sediment motion in SRD

Also, the increase of effective Shields Number θ' reflects higher shear stress, which correlates with a rise in suspended sediment concentration.

Overall, a steeper upstream slope leads to significant velocity changes and locally higher shear stress, which promotes greater sediment suspension, reduces the likelihood of sediment deposition and

increase the risk of bed scour.

4. Conclusion

4.1. Optimization channel

- 1) Under conditions of long-term average discharge and water levels, the optimized channel exhibits a lower peak value relative error (σ) and demonstrates greater stability compared to the natural channel.
- 2) During a 100-year return period storm event, the correlation coefficient for the optimized channel exceeds 0.8, indicating stronger performance in extreme conditions. Overall, the optimized channel outperforms the natural channel in handling such extreme scenarios.

4.2. Suitable Shape of Trapezoidal-Board Weir

Based on the comparison of different weir designs in terms of flow dynamics and sedimentation in Table. 5, the following conclusions can be drawn:

- 1) The design of the weir crest successfully prevents the formation of undular flow.
- 2) Flow over the weir generally follows a parallel streamline, ensuring a smooth transition.
- 3) To accommodate a higher flow capacity, a mild upstream slope is preferable, as it enhances flow efficiency.
- 4) A steeper upstream slope increases shear stress near the downstream heel, significantly raising the potential for erosion in that area.
- 5) From a stability perspective, a steeper upstream slope positively influences overall flow stability.

Table. 5 Analysis of Hydraulic Performance for Various Weir Slopes

Weir	Flow Condition	Velocity distribution	Turbulence	Sediment transport
No. 1 $\theta=27^\circ$ Mild Slope	1) No undular flow; 2) Parallel streamline.	1) Relatively lower averaged velocity magnitude; 2) High vertical velocity may damage hydraulic structures.	Largest range of turbulence.	Stable sheart stress, reduces suspension sediment transport.
No. 2 $\theta=54^\circ$ Moderate Slope	Too high Fr values	-	-	
No. 3 $\theta=74^\circ$ Steep Slope	1) Smoother and flatter water profile; 2) Hydraulic jump shifts far downstream from the weir heel.	1) Reduces discharge coefficient C_D ; 2) Minimum vertical velocity and low average velocity magnitude.	Smallest range of turbulence	Higher shear stress increases the likelihood of downstream erosion.

References

- [1] S. E. Greco and E. W. Larsen, 'Ecological design of multifunctional open channels for flood control and conservation planning', *Landscape and Urban Planning*, vol. 131, pp. 14–26, Nov. 2014, doi: 10.1016/j.landurbplan.2014.07.002.
- [2] Y. Jia, 'Minimum froude number and the equilibrium of alluvial sand rivers', *Earth Surf. Process. Landforms*, vol. 15, no. 3, pp. 199–209, May 1990, doi: 10.1002/esp.3290150303.
- [3] Z. Cui and X. Zhang, 'FLOW AND SEDIMENT SIMULATION AROUND SPUR DIKE WITH FREE SURFACE USING 3-D TURBULENT MODEL'.
- [4] Shenzhen Water Bureau, 'Preliminary Design Report on River Training in Shawan River Basin of Shenzhen', Sep, 2015.
- [5] DHI MIKE User Manual.
- [6] M. R. Madadi, A. Hosseinzadeh Dalir, and D. Farsadizadeh, 'Investigation of flow characteristics above trapezoidal broad-crested weirs', *Flow Measurement and Instrumentation*, vol. 38, pp. 139–148, Aug. 2014, doi: 10.1016/j.flowmeasinst.2014.05.014.
- [7] 'FLOW-3Dv11.0.pdf'.
- [8] J. Fredsøe and R. Deigaard, *Mechanics of Coastal Sediment Transport*, vol. Volume 3. in Advanced Series on Ocean Engineering, no. Volume 3, vol. Volume 3. WORLD SCIENTIFIC, 1992. doi: 10.1142/1546.
- [9] E. Sidiropoulos, K. Vantas, V. Hrissanthou, and T. Papalaskaris, 'Extending the Applicability of the Meyer–Peter and Müller Bed Load Transport Formula', *Water*, vol. 13, no. 20, Art. no. 20, Jan. 2021, doi: 10.3390/w13202817.
- [10] R. A. Gaines and R. H. Smith, 'Micro-Scale Loose-Bed Physical Models', in *Hydraulic Measurements and Experimental Methods 2002*, Estes Park, Colorado, United States: American Society of Civil Engineers, Oct. 2002, pp. 1–12. doi: 10.1061/40655(2002)78.
- [11] M. H. García, 'The Legend of A. F. Shields'.
- [12] 'PUB_COP_7th_Edition in Singapore.pdf'. Accessed: Oct. 09, 2023. [Online]. Available: https://www.pub.gov.sg/Documents/PUB_COP_7th_Edition.pdf
- [13] O. Castro-Orgaz and H. Chanson, 'Near-critical free-surface flows: real fluid flow analysis', *Environ Fluid Mech*, vol. 11, no. 5, pp. 499–516, Oct. 2011, doi: 10.1007/s10652-010-9192-x.
- [14] H. M. Fritz and W. H. Hager, 'Hydraulics of Embankment Weirs', *Journal of Hydraulic Engineering*, vol. 124, no. 9, pp. 963–971, Sep. 1998, doi: 10.1061/(ASCE)0733-9429(1998)124:9(963).
- [15] M. H. Chaudhry, *Open-Channel Flow*. Cham: Springer International Publishing, 2022. doi: 10.1007/978-3-030-96447-4.

Appendix-I: Bedload and Suspended Sediment Analytical Solutions

```
%% shields parameter
theta_V1 = V1_Uf_filtered(:,2).^2/(s-1)/g/d;

% if statement for the lower or upper regime
theta_prime_spe1 = 0.06 + 0.3*theta_V1.^1.5; % for theta_prime <= 0.55, lower regime

for i=1:length(theta_prime_spe1)
    theta_prime_spe = theta_prime_spe1(i);
    theta_spe = theta_V1(i);
    if theta_prime_spe > 0.55 % upper regime
        theta_prime_spe = (0.702*theta_spe^(-1.8)+0.298)^(-1/1.8); % for theta_prime > 0.55, upper regime
    end
    theta_prime_spe1(i) = theta_prime_spe;
end

%% MPM for Bedload transport rate: qB (m2/s)
% phiB_MPM = 8.*(theta_prime - theta_cri).^1.5;
% qB_MPM = phiB_MPM* sqrt((s-1)*g*d^3);

% Re, d = grain size
% theta_cri: explicit formular of Critical Shield Paramter
Re_spe1 = V1_Uf_filtered.*d/vi;
theta_cri_spe1 = 0.165*(Re_spe1 + 0.6).^(-0.8)+0.045*exp(-40.*Re_spe1.^-1.3);

for i=1:length(theta_prime_spe1)
    theta_prime_spe = theta_prime_spe1(i);
    theta_cri_spe = theta_cri_spe1(i);
    phiB_MPM = 8*(theta_prime_spe - theta_cri_spe)^1.5;
    qB_MPM = phiB_MPM* sqrt((s-1)*g*d^3);
    qB_spe1(i) = qB_MPM;
end

%% show 2 y-axis
figure(1)
% Left y-axis: Bedload Transport Rate
yyaxis left
semilogy(V1_Uf_filtered(:,1), qB_spe1, 'r-', 'MarkerSize', 12, 'LineWidth', 2);
hold on;
ylabel('Bedload Transport Rate (MPM method) qB (m^2/s)');
grid on;

% Right y-axis: Shear Velocity Uf
```

```
yyaxis right
plot(V1_Uf_filtered(:,1), V1_Uf_filtered(:,2), 'r--', 'MarkerSize', 12, 'LineWidth', 2);
hold on;
ylabel('Shear Velocity Uf (m/s)');
% Common x-axis label
xlabel('y direction (m)');
% Title and legend
title('Bedload Transport Rate and Friction Velocity along Flow Direction');
legend({'V1 (qB)', 'V2 (qB)', 'V3 (qB)', 'V1 (Uf)', 'V2 (Uf)', 'V3 (Uf)'}, 'Location', 'best');
% Font size adjustment
set(gca, 'FontSize', 14);
% Additional grid settings (optional for clarity)
grid on;
```